J Artif Organs (2002) 5:91–96

ORIGINAL ARTICLE

Kenji Shiba, DEng · Kohji Koshiji, DEng
Eisuke Tatsumi, MD, PhD
Yoshiyuki Taenaka, MD, PhD
Hisateru Takano, MD, PhD

Analysis of specific absorption rate in biological tissue surrounding transcutaneous transformer for an artificial heart

Abstract This paper reports on specific absorption rate (SAR) analysis of biological tissue surrounding a transcutaneous transformer for an artificial heart. An externally coupled type of transformer was used for transcutaneous energy transmission. The secondary (internal) coil of the transformer, which is covered with skin, protrudes from the body surface, forming a skin tunnel. A primary (external) coil closely wound around a toroidal ferrite core is inserted into the skin tunnel. In this transformer, most of the magnetic flux induced by the current of the primary coil is linked with the secondary coil, and the coupling factor between the primary and secondary coils is greater than 0.98, regardless of the skin thickness. The electromagnetic field in the biological tissue surrounding the transformer was analyzed by the transmission line modeling method, and the distributions of the electric field strength and the SAR as a function of output power, the number of coil loops, and the dimensions and output voltage of the transcutaneous transformer were estimated. We found that SARs near the transcutaneous transformer were larger than at other points, that is, the SARs far from the transformer were relatively small. It was also clear that by increasing the dimensions and number of coil loops, and reducing the output voltage, we could reduce the SAR in biological tissue surrounding the transcutaneous transformer. The SAR in the present study was within the limits recommended by the Ministry of Posts and Telecommunications of Japan.

Received: March 21, 2001 / Accepted: December 27, 2001

K. Shiba (✉) · K. Koshiji
Department of Electrical Engineering, Faculty of Science and Technology, Tokyo University of Science, 2641 Yamazaki, Noda 278-8510, Japan
Tel. +81-4-7124-1501 (ext.3743); Fax +81-4-7120-1741
e-mail: shiba@ee.noda.sut.ac.jp

E. Tatsumi · Y. Taenaka · H. Takano
Department of Artificial Organs, National Cardiovascular Center Research Institute, Suita, Japan

Key words Artificial heart · Energy transmission · Transformer · SAR · TLM method

Introduction

In terms of quality of life and resistance to infection, transcutaneous energy transmission (TET)[1–8] is the most promising method for supplying the energy to power an implanted total artificial heart.[1] We have been developing the externally coupled transcutaneous energy transmission system (ECTETS)[2–8] and have obtained high-energy transmission efficiency of greater than 98% between the internal and external coils, with high stability.[3–8]

To make this method practical, we must investigate the electromagnetic influence of TET on biological tissue (EMB)[9–11] and its electromagnetic interference (EMI)[7–9] with other electronic equipment. Although we have already investigated EMI[7,8] from the ECTETS and confirmed its safety, the only evaluation of EMB has been made by using a coreless type of transcutaneous transformer.[2]

Electromagnetic influences on biological tissue include thermal effects, stimulant action, and nonthermal effects.[9–11] This paper reports on the thermal effect caused by the electromagnetic wave due to transcutaneous transmission using the ECTETS. Specific absorption rate (SAR, W/kg), which is often used as an index of the thermal effect, is defined as the power of an electromagnetic wave absorbed into biological tissue per unit mass of 1 kg. In this paper, SAR in the biological tissue surrounding the externally coupled type of transcutaneous transformer is analyzed by transmission line modeling (TLM)[12,13] and compared with the guidelines[9,10] established by the Japanese Ministry of Posts and Telecommunications.

Construction of the TET system and externally coupled transcutaneous transformer

Figure 1 shows a block diagram of the TET system. A maximum rating power of 40 W in the TET system is re-

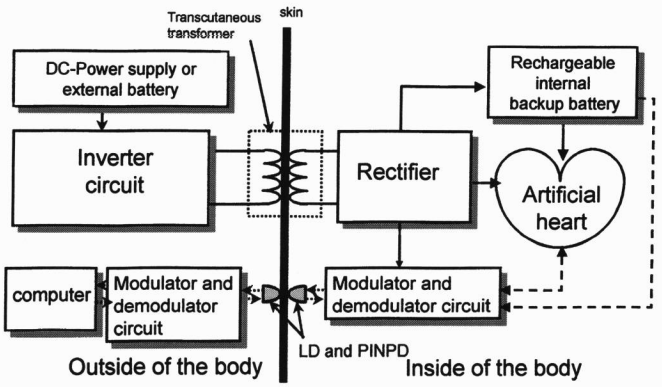

Fig. 1. Block diagram of the transcutaneous energy transmission (TET) system. *LD*, Laser diodes; *PINPD*, PIN photodiodes

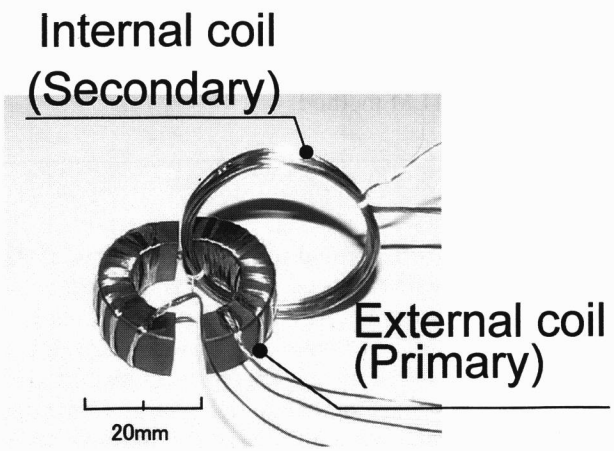

Fig. 2. Externally coupled transcutaneous transformer

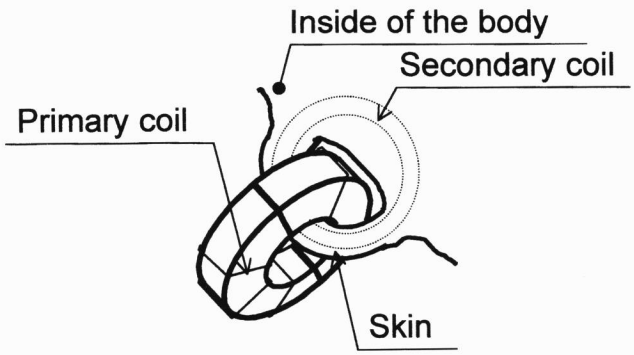

Fig. 3. Externally coupled transcutaneous transformer attached to the body

quired to power a totally artificial heart.[1] Figures 2 and 3 show external views of an externally coupled type of transcutaneous transformer used for a TET system. A secondary (internal) coil covered with skin, whose diameter is about 40 mm, protrudes from the body surface, forming a skin tunnel. A primary (external) coil tightly wound around a toroidal ferrite core is inserted into the skin tunnel. In this transformer, because most of the magnetic flux induced by the current of the primary coil is linked with the secondary coil, the coupling factor between the primary and secondary coils is greater than 0.98,[5,7] regardless of the skin thickness.

Methods

Estimation of SAR

SAR is expressed by Eq. 1:

$$\mathrm{SAR} = \frac{\sigma E^2}{\rho}[\mathrm{W/kg}] \tag{1}$$

where E is the root mean square of the electric field (V/m), σ is the electric conductivity of biological tissue (S/m), and ρ is the density of biological tissue (kg/m^3). SAR is evaluated by two methods,[9,10] one experimental and one analytical. In the experimental method, the electric field in a liquid phantom is measured, but it is very difficult to make a liquid phantom with a complicated structure like the human body. The second method, which is much easier to use, analyzes the distribution of electromagnetic fields. In this paper, SAR is numerically analyzed using TLM.

TLM models are very powerful tools for field computations.[12,13] They are based on an analogy between the electromagnetic field and the grid of transmission lines. A mathematical derivation of the TLM method can be directly obtained from a full wave time-domain solution to Maxwell's equations. The theory and application of TLM for electromagnetic simulation are reviewed by Hoefor.[14]

Model for numerical analysis

A model for numerically analyzing SAR in the biological tissue surrounding the transcutaneous transformer is shown in Fig. 4a and b. Figure 4b shows the inside of the model with the upper part removed. It is assumed that the transcutaneous transformer (100 × 95 × 60 mm) attached to the body is placed in a realm (160 × 160 × 80 mm) with an intrinsic impedance of 377 Ω that perfectly absorbs the electromagnetic wave.

The primary coil with N_1 loops is closely wound around a toroidal ferrite core with outer and inner diameters of 38 and 22 mm, respectively, and a thickness of 14 mm. In the present study, the number of loops in the secondary coil, N_2, which was equal to N_1, ranged from 6 to 12; the diameter of the secondary coil was 40 mm; and the thickness of the coil was 9.5 mm. The coil also had a silicone coating 3.5 mm in thickness. As shown in Figs. 2 and 3, the secondary coil is implanted into the body, and half of it is covered with skin (a thickness of 3 mm) and protrudes like an arch.

These dimensions were determined according to the results of our animal experiments.[3–7] Table 1 shows the electrical properties of the ferrite core, silicone, and biological tissue[11] used in this paper. Here, an average value of 1000 kg/m^3 was used to represent the density of biological tissue consisting of fat, bone, and skin.[15] The model for numerical analysis by TLM had grids of 0.37 to 2.5 mm in

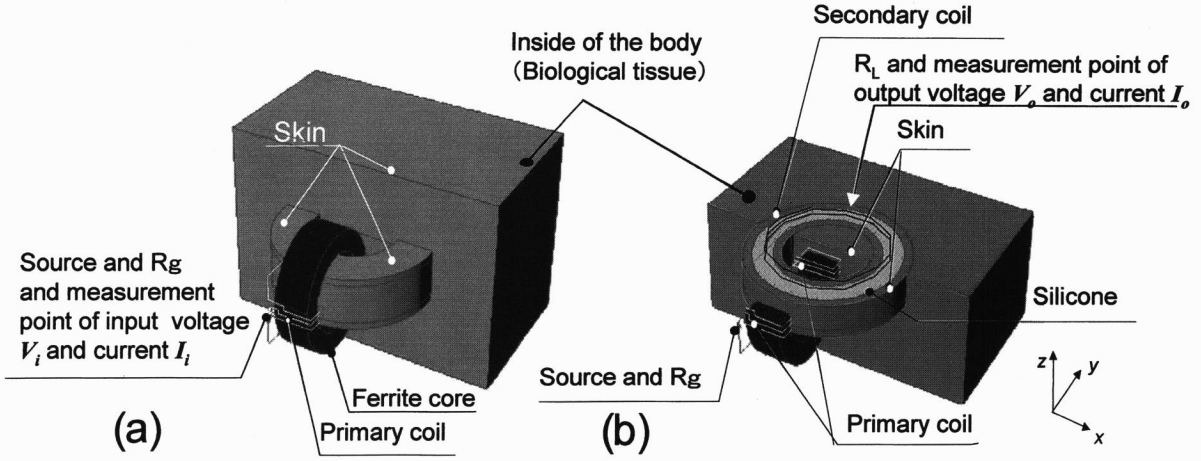

Fig. 4. Analyzed model

Table 1. Electrical properties of ferrite core, silicone, and biological tissue used in the analysis

Material	Relative permeability	Relative permittivity	Conductivity (S/m)
Ferrite core	4100	1	0
Silicone	1	3	0
Biological tissue	1	30000	0.5

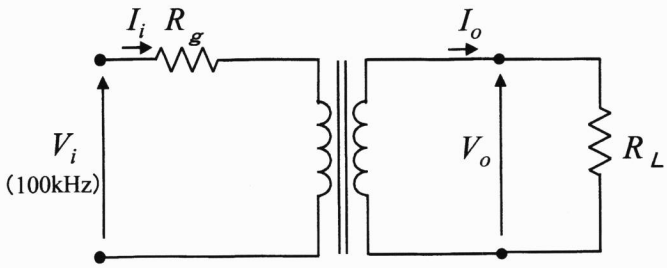

Fig. 5. Equivalent circuit

the vicinity of the coil, and from 2.5 to 7.0 mm in the other regions.

Figure 5 shows an equivalent circuit of the transcutaneous transformer. A sinusoidal wave source of 100 kHz with output voltage V_i and resistance R_g was applied to the terminal of the primary coil. The magnitude of V_i was adjusted to remain constant at a load voltage of 24 V. A load resistance R_L electrically simulating an artificial heart was connected to the terminal of the secondary coil.

Analysis of voltages, currents, and SAR as a function of output power

The input voltage V_i, input current I_i, output voltage V_o, and output current I_o of the transcutaneous transformer and the electric field distribution surrounding the transcutaneous transformer were obtained as a function of output power from the analysis. Then V_i, I_i, V_o, and I_o were compared with the respective values of a real model that has the same size, shape, and electromagnetic parameters as the analyzed model. Figure 6 shows a block diagram of the measurement system. A sine wave generator (HP, 33120A), a high-speed amplifier (NF, 4025), a high-frequency digital power meter equipped with voltage and current meters (Yokogawa, PZ4000), transcutaneous transformer, and noninductive resistances are used.

The toroidal core of the transcutaneous transformer is made from Mn-Zn ferrite with a relative permeability of 3000–5000, and the coils are wound with ø 0.1-mm polyurethane-coated copper litz wire (30 wires bundled).

At present, it is very difficult to measure SAR by an in vivo experiment to verify the analyses. Hence, we indirectly show the validity of results obtained from the SAR analyses, comparing the voltages V_i and V_o and the currents I_i and I_o obtained from the analyses with those from measurements in the transcutaneous transformer. In this paper, "Micro-Stripes" (KCC, Tokyo, Japan), the electromagnetic simulator, employing the TLM method, is used to analyze V_i, I_i, V_o, I_o, and the electric field distribution. SARs were then estimated from the electric field distribution obtained from the above analysis and Eq. 1.

Analysis of SAR as a function of the number of coil loops

Equating the number of loops of the primary coil N_1 to that of the secondary coil N_2 ($N = N_1 = N_2$), the SARs were analyzed as a function of the number of coil loops (from 6 to 12) under the conditions of an output power of 40 W and a voltage of 24 V. A model consisting of $N = 10$ loops with an output power of 40 W and an output voltage of 24 V was the standard model. The results obtained from analyses of various models were compared with the results of the standard model.

Analysis of SAR as a function of dimension

A model in which the dimensions of the transcutaneous transformer were multiplied by 0.75 was analyzed, and miniaturization of the transformer was investigated.

Fig. 6. Block diagram of measurement system

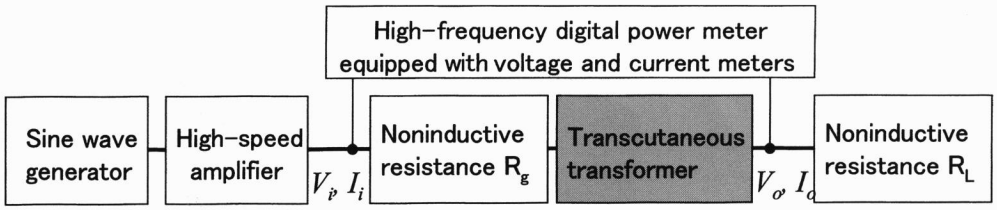

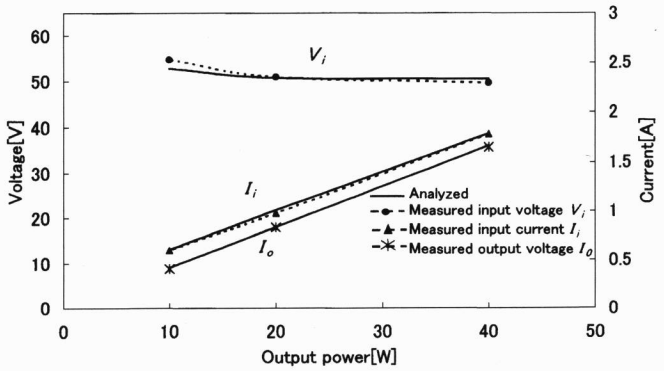

Fig. 7. Results obtained from analysis and measurement of voltages and currents as a function of output power of ECTETS

Analysis of SAR as a function of output voltage

Reduction of the output voltage allows the number of rechargeable internal batteries[6,7] to be reduced. A model in which the output voltage was multiplied by 0.5 was analyzed and compared with the standard model.

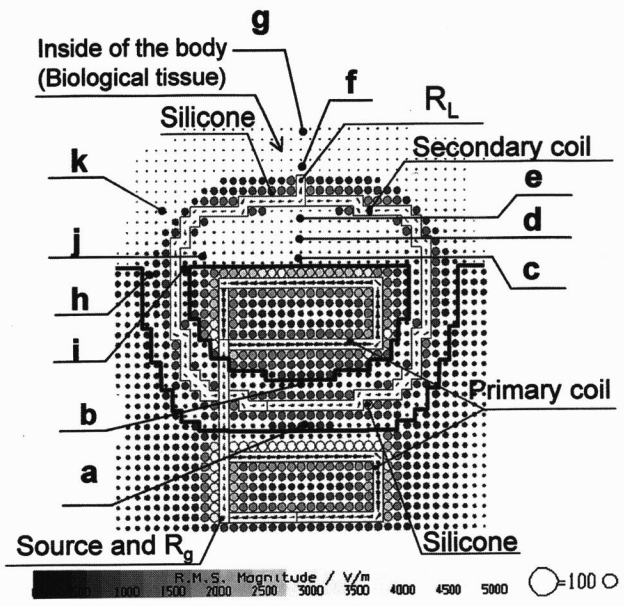

Fig. 8. Electric field distribution in the tissue surrounding the transcutaneous transformer

Results

Analysis of voltages, currents, and SAR as a function of output power

Figure 7 shows a comparison of the analytical results with the measured data as a function of output power in case of an output voltage V_o of 24 V, verifying the validity of the analysis. Figure 8 shows the electric field distribution obtained from the analysis (N = 6 loops, output power 40 W, and output voltage 24 V). Figure 9 shows the analyzed SARs at points from *a* to *k* as a function of output power from 10 to 40 W.

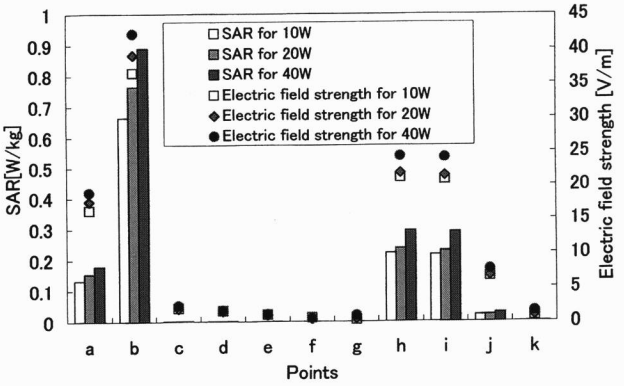

Fig. 9. Specific absorption rate (SAR) in the tissue surrounding the transcutaneous transformer as a function of output power

Analysis of SAR as a function of the number of coil loops

Figure 10 shows SAR at points from *a* to *k* as a function of the number of coil loops.

Analysis of SAR as a function of dimension

Figure 11 shows SAR at each point from *a* to *k* using the transformer scaled down by 0.75.

Analysis of SAR as a function of output voltage

Figure 12 shows SAR at each point from *a* to *k* as a function of output voltage.

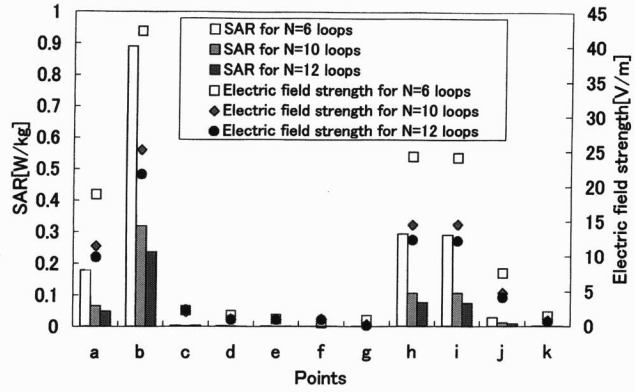

Fig. 10. SAR in the tissue surrounding the transcutaneous transformer as a function of the number of coil loops

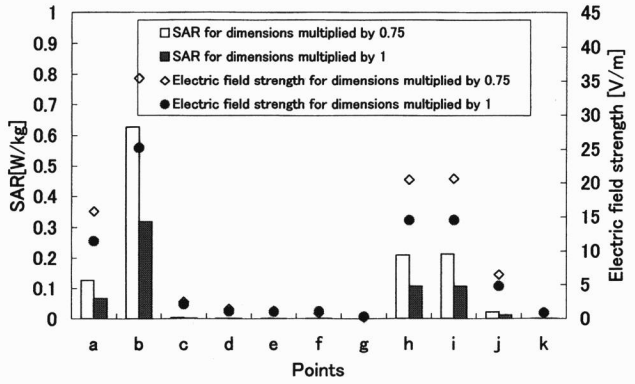

Fig. 11. SAR in the tissue surrounding the transcutaneous transformer as a function of dimension

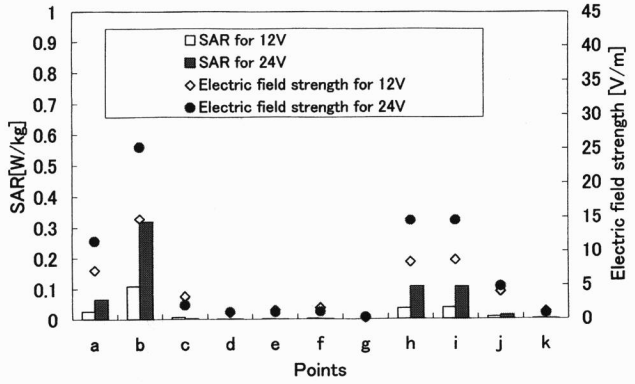

Fig. 12. SAR in the tissue surrounding the transcutaneous transformer as a function of output voltage

Discussion

Analysis of SAR and the voltages and currents as a function of output power

Figure 7 shows that the analytical results agree fairly well with the actual measurements. As for the other models including the standard model, comparing V_i, I_i, and I_o in the analyses with the respective values in the measurements, we found that the errors between them were negligibly small, within 5%. This shows that our analysis is correct. In Figs. 8 and 9, we can see that the SARs at points *a*, *b*, *h*, and *i* were larger than at the other points. The SARs at points *f* and *g* were much smaller, because these points were far from the transcutaneous transformer. Figure 9 also shows that the SARs at points *a*, *b*, *h*, and *i* were multiplied by 1.06 to 1.35 when the output power was increased 2 to 4 times.

Assuming that the shape of the biological tissue in the vicinity of the transcutaneous transformer is a cylindrical ring with a diameter of 40 mm, we made a simple computation of the electric field in the ring, equal to a one-loop coil, induced by the primary coil. The electric field along a six-loop secondary coil was computed as 24/6/0.126 (with 24 being equal to the electromagnetic motive force in volts, and 0.126 equal to the total length of the secondary coil in meters). The resultant electric field had a magnitude of 31.7 V/m and is nearly of the magnitude of the field numerically analyzed by TLM in this paper (corresponding to the average of electric field strength at points *a*, *b*, *h*, and *i* in Fig. 9).

The magnetic flux ø induced by the primary coil is expressed as

$$\phi = \frac{V_o}{4.44 N_2 \cdot f}[\mathrm{Wb}] \tag{2}$$

where the frequency f, the output voltage V_o, and the number of loops of secondary coil N_2 are independent of the output power, making the electric field and SAR also independent of it.

The increment in SAR proportional to the output power in Fig. 9 was caused by the increment in magnetic flux compensating the voltage drop due to the leakage induced by the secondary coil.

Analysis of SAR as a function of the number of coil loops

In Fig. 10, we can see that the SARs at points *a*, *b*, *h*, and *i* in the case of $N = 6$ loops were 2.46 to 2.80 times higher than the respective values in the standard model (1.57 to 1.67 times for electric field distribution). In contrast, SARs at points *a*, *b*, *h*, and *i* in the case of $N = 12$ loops were 70% to 74% of the values in the standard model (0.83 to 0.86 times for electric field distribution). SAR and the electrical field both decreased as the number of coil loops increased.

From the preceding section, the electric field E along the secondary coil of N' loops is computed as

$$E = \frac{V_o}{N' \cdot l} \tag{3}$$

(with V_o being equal to the electromagnetic motive force in volts and l equal to the total length of the secondary coil). From Eq. 3, as the number of coil loops was changed from N' to N'', the electric field along the secondary coil had to be

multiplied by N'/N''. When the number of coil loops changed from 10 to 6, the flux had to be multiplied by 10/6, in comparison with the standard model. We found that the electric field was nearly equal to 10/6 times the value of the standard model in our analysis, and the resultant field was quite similar to that in Eq. 3. Identical results were obtained for $N = 12$.

Analysis of SAR as a function of dimension

In Fig. 11, the dimensions of the transformer were scaled down by 0.75, making SAR at points *a*, *b*, *h*, and *i* about 1.90 to 2.01 times higher than the respective values in the standard model (1.38 to 1.42 times for electric field distribution). SAR increased as the dimensions of the transformer decreased.

Since the dimensions of the transformer are multiplied by x, the resultant electric field is divided by x, because the dimensions of the transformer are proportional to the total length of the coil, and from Eq. 3 the electric field strength is inversely proportional to the total length of the coil.

It can also be seen in Fig. 11 that when the dimensions were scaled down by 0.75, the field had to be multiplied by $1/0.75 = 1.33$.

Analysis of SAR as a function of output voltage

In Fig. 12, as the output voltage was reduced by 0.5, SAR at points *a*, *b*, *h*, and *i* was reduced by 0.32 to 0.38 compared with the respective values in the standard model (electric field reduced by 0.56 to 0.61). This is because the output voltage was proportional to the electric field in Eq. 3.

From these results, we found that by increasing the number of loops and dimensions of the coils and reducing the output voltage, we could reduce SAR in biological tissue surrounding the transcutaneous transformer.

Because the SARs analyzed in this paper were within the values of the SAR guidelines[9,10] of 8 W/kg established by the Japanese Ministry of Posts and Telecommunication, the externally coupled transcutaneous energy transmission was safe in terms of thermal effect.

Conclusions

The results obtained from the analysis agreed fairly well with the measured values. Thus, we concluded that our analysis could be used to estimate SAR in the biological tissue surrounding the transcutaneous transformer. Further, we found that SAR in the vicinity of the transformer was sufficiently small for a transcutaneous energy transmission of 40 W, below the SAR guidelines established by the Japanese Ministry of Posts and Telecommunications, and its thermal effect caused by the electromagnetic wave was insignificant.

Acknowledgments This work was partly funded by a government grant for promoting scientific research.

References

1. Masuzawa T, Tastumi E, Taenaka Y, Nakamura M, Endo S, Takano H, Koshiji K, Fukui Y, Tsukahara K. Progress of an electrohydraulic total artificial heart system with a separate energy converter. ASAIO J 1999;45:471–477
2. Koshiji K, Nomura T, Komori T, Yuzawa Y, Masuzawa T, Shu E, Utsunomiya T, Masuzawa T, Taenaka Y, Takano H. About the radiated emission from transcutaneous energy transmission system and its repression. IEE Japan 1991;MAG-91-239,LD-91-74:19–26
3. Shiba K, Shu E, Koshiji K, Tsukahara K, Tsuchimoto K, Ohu-mi T, Nakamura T, Endo S, Masuzawa T, Tatsumi E, Taenaka Y, Takano H. Efficiency improvement and in vivo estimation of externally-coupled transcutaneous energy transmission system for a totally implantable artificial heart. Proceedings 19th International Conference IEEE/Engineering in Medicine and Biology Society 1997:2503–2505
4. Shiba K, Shu E, Koshiji K, Tuchimoto K, Tsukahara K, Masuzawa T, Kakuta Y, Tatsumi E, Taenaka Y, Takano H. Externally coupled transcutaneous energy transmission system for a totally implantable artificial heart – in vitro and in vivo estimations from the viewpoint of electrical engineering. Jpn J Artif Organs 2000; 29:24–30
5. Shiba K, Shu E, Koshiji K. Analysis of externally-coupled transcutaneous transformer for a totally-implantable artificial heart. Transaction of the Institute of Electrical Engineers of Japan 2000;120:169–175
6. Shiba K, Shu E, Koshiji K, Tsukahara K, Tuchimoto K, Masuzawa T, Tatsumi E, Taenaka Y, Takano H. A transcutaneous energy transmission system with rechargeable internal back-up battery for a totally implantable total artificial heart. ASAIO J 1999;45:446–470
7. Shiba K. A study of transcutaneous energy transmission system for an implantable artificial heart. Doctoral thesis, Science University of Tokyo, 2000
8. Matsubara H, Shiba K, Koshiji K, Fujiwara O, Nakamura Y, Tatsumi E, Taeneka Y, Takano H. Transcutaneous energy transmission system for a totally implantable artificial heart – measurement and evaluation of electromagnetic disturbance. Jpn J Artif Organs 2000;29:18–23
9. Nitta S, Kami Y, Sato Y, Sugiura K, Seto N, Fujiwara O. Electromagnetic compatibility handbook. Tokyo: Asakura Publishers, 1999
10. ARIB Standard (Radiofrequency-Exposure Protection, RCR STD-38-2). Tokyo: Association of Radio Industries and Businesses, 1999
11. Reilly JP, Antoni H, Chilbert MA, Sweeney JD. Applied bioelectricity. New York: Springer, 1998;17–18
12. Christos C. The transmission-line modeling method. New York: IEEE Press, 1995
13. Krumpholz M, Russer P. A field theoretical derivation of TLM. IEEE Trans Microwave Theory Tech. 1994;42:1660–1668
14. Hoefor WJR. The transmission-line modeling method – theory and applications. IEEE Trans Microwave Theory Tech. 1985; MTT-33:882–893
15. Japan Society of Medical Electronics and Biological Engineering. Handbook of clinical engineering. Tokyo: Corona Publishers, 1984;113